Current-current correlations in a model CuO_3 system

Bhargavi Srinivasan and Marie-Bernadette Lepetit

Laboratoire de Physique Quantique, UMR 5626 du CNRS, Université Paul Sabatier, F-31062 Toulouse Cedex 4, France

(February 1, 2008)

We study a 3-band extended Hubbard model on a CuO_3 system by the density matrix renormalization group (DMRG) method. Our system has geometry similar to that of a section of the CuO_2 plane of the copper-oxide superconductors. We have studied the effects of nearest-neighbour repulsions on the current-current correlations of two model CuO_3 systems. We have calculated several types of staggered current correlations as a function of various model parameters such as interaction strengths and filling. We show that repulsive interactions are clearly capable of increasing the magnitude of the current-current correlations in both models studied. The long-distance behavior of the current-current correlations is qualitatively influenced by V. We show that repulsive interactions are capable of enhancing correlations involving at least one copper-oxygen rung over distances comparable to the length of the system. In some cases, V decreases the exponent corresponding to the power-law decay, leading to a considerable slowing down of the long-distance decay of the current-current correlations, compared to that of the Hubbard model.

PACS numbers: 71.10.Fd, 71.10Hf, 74.20Mn

I. INTRODUCTION

The unusual normal-state phenomenology of the high T_c superconductors constitutes an important theoretical challenge since there is not yet a consensus in the community about a consistent microscopic theory that would reproduce all aspects of the phase diagram of the cuprates. Angle-resolved photoemission spectroscopy (ARPES) experiments have revealed several properties of the so-called pseudogap phase in the underdoped part of the phase diagram [1] and it is likely that this phase holds the key to a general understanding of the phase diagram. Among the scenarios proposed to explain the pseudogap phase, we mention the 'circulating-current' order-parameter, which breaks time-reversal symmetry and four-fold rotational symmetry about the copper atoms, while preserving the translational symmetry of the lattice [2]. This theory also gives rise to non-Fermi liquid behaviour. The 'd-density wave' (DDW) order-parameter based on orbital currents [3] has been proposed as a hidden order parameter for the phase diagram of the cuprates. In Fig. 1 we present a schematic picture of these circulating currents in the CuO_2 plane of the copper-oxides.

Phases similar to those with DDW or circulating-currents order-parameters have been discussed previously in the literature under different guises. The so-called orbital antiferromagnet is a phase with broken translational and time-reversal symmetries, described for the excitonic insulator [4] and in the two-dimensional (2D) Hubbard model [5]. 'Flux phases' were studied in the context of the large n limit of the Heisenberg model [6]. Staggered currents were found to be stabilized by attractive nearest-neighbour interactions in the 2D Hubbard model [7]. On the other hand, $t - J$ clusters [8,9] were shown variationally and numerically to have a staggered flux

order-parameter. Recently, the doped two-leg $t - J$ ladder, studied by the density matrix renormalization group (DMRG) method [10] was found to have exponentially decaying rung-rung current-current correlations. However, the staggered flux phase was found to be stabilized in the half-filled 2-leg ladder by abelian bosonization methods [11]. Further, inclusion of longer-range interactions in the 2-leg ladder (extended $t - U - V - J$ model) appears to stabilize the staggered flux phase, as seen from DMRG calculations [12].
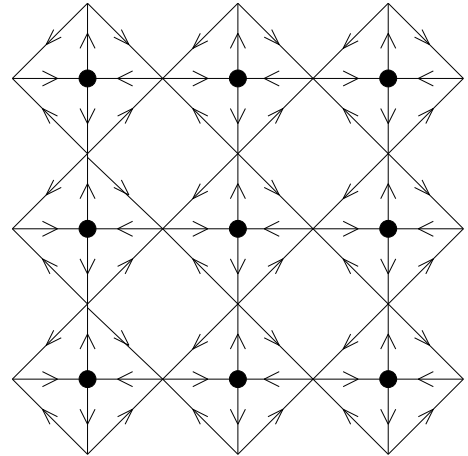

FIG. 1. Schematic picture of the circulating-current phase in the copper-oxides. The filled circles represent copper atoms and the vertices oxygen atoms of the CuO_2 plane. The arrows on each bond correspond to the direction of the current along the bond.

With this collection of stimulating results on flux phases in the Hubbard and $t - J$ models, it would be interesting to study a system whose geometry more closely resembles that of the copper-oxides. This is especially relevant in the light of the debate regarding the suitabil-

ity of the $t-J$ model to the copper-oxide system and in particular the importance of an explicit treatment of the oxygen atoms [13]. There is now general agreement in the community that the CuO_2 planes play a crucial role in the high T_c superconductors [13] and that the geometry of the copper-oxides is relevant to superconductivity. Further, several models with effective interactions have been proposed to describe the CuO_2 plane [14,15,13]. These studies have emphasized the role of strong electronic correlations. Mean-field studies [2] have indicated that it is necessary to go beyond on-site interactions and an explicit treatment of the nearest-neighbour interactions is necessary to stabilize the circulating-current phase. An accurate treatment of the strongly correlated full 2D CuO_2 system, though desirable, is not presently forthcoming. Therefore, we have opted for a CuO_3 system that we believe to incorporate the crucial geometric ingredients of the system, including an explicit treatment of oxygen sites, which can then be studied by the highly accurate DMRG method [16].
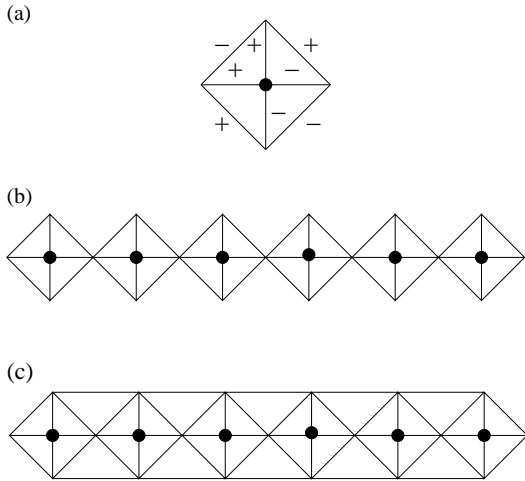
(a)

(b)

(c)

FIG. 2. (a) Single unit cell of the CuO_3 system studied, the copper site is marked by a filled circle and all vertices correspond to oxygen sites. The phase conventions of the transfer integrals, corresponding to the symmetry of the d- and p-orbitals are indicated (b) Model 1 : 6 unit cells of the extended CuO_3 system with $t_\parallel = 0$ (c) Model 2 : similar to (b) with $t_\parallel \neq 0$.

In this paper we study currents in a 3-band extended Hubbard Hamiltonian on a CuO_3-type system (Fig. 2), which is believed to model the essential aspects of the 2D system. It is possible to envisage several quasi-1D sections of the 2D CuO_2 plane. It is necessary to choose geometries that are capable of supporting circulating currents. The plaquette that forms a single unit cell of the CuO_2 plane is shown in Fig. 2a. The system shown in Fig. 2b, henceforth to be called Model 1, consists of such plaquettes connected at a single point ($t_\parallel = 0$). A strip of the CuO_2 plane is shown in Fig. 2c. In this system,

henceforth known as Model 2, links parametrized by $t_\parallel$ have been added between adjacent plaquettes to model the 2D nature of the system. This is expected to better correspond to scenario in the CuO_2 planes where the plaquettes are all coupled due to hopping along both axes.

The essential difference between models 1 and 2 is that since the plaquettes of Model 1 are connected at just a single point, it is possible to globally reverse the signs of the currents in each unit-cell completely independently of all the other unit-cells, without any energy cost. Therefore, while each unit-cell is a-priori capable of sustaining currents, long range order is not possible in Model 1. Thus, it would be necessary to include links between these plaquettes (present in the physical system), a scenario which corresponds to Model 2. In this paper, we have examined both these models in detail in order to study the effects of interactions locally in a single unit cell as well as the long-range effects brought about by coupling plaquettes as in Model 2.

For weak interactions, ladder-type systems can be treated using a combination of bosonization and perturbative renormalization group techniques, as in the case of the 2-leg ladder (with disorder) [17] or N-leg Hubbard ladder [18]. In fact, abelian bosonization methods have been used to study staggered currents in the 2-leg ladder [11]. These powerful analytical tools have proved useful in extracting a great deal of information. However, these methods cannot fully take into account the exact values of the parameters as well as the precise geometry of the system, both of which are crucial to the copper-oxides as discussed above. While our system appears to be a quasi-1D system, it has a highly non-trivial geometry and up to 4th neighbours are connected. Given the large number of parameters in the 3-band Hubbard model and the importance of the delicate balance between them, we have chosen to use the highly accurate DMRG method which gives information even in the strong-coupling regime inaccessible to perturbative approaches.

We have used a 3-band extended Hubbard model on the systems in Fig. 2, described in greater detail below. The 3-band Hubbard model for clusters of the CuO_2 system (up to 6×6 unit-cells) has been studied by the constrained path quantum Monte Carlo method (CPMC) [19,20]. However, the focus of the CPMC studies was pair-binding of holes as well as the pairing and other correlation functions, but not currents. Thus, a study of flux-type phases or currents in this model does not exist, to our knowledge.

II. MODEL AND METHOD

The 3-band Hamiltonian for our CuO_3 system in the hole picture is given by:

$$H = H_0 + H_1 + H_2 \tag{1}$$

$$H_0 = \Big[\sum_{i,\sigma} -t_{pd} d^\dagger_{i\sigma}(p_{x,i+a/2,\sigma} - p_{x,i-a/2,\sigma} - p_{y,i+a/2,\sigma}$$

$$+ p_{y,i-a/2,\sigma}) - t_{pp} p^\dagger_{x,i+a/2,\sigma}(-p_{y,i+a/2,\sigma} + p_{y,i-a/2,\sigma}) -$$

$$t_{pp} p^\dagger_{x,i-a/2,\sigma}(p_{y,i+a/2,\sigma} - p_{y,i-a/2,\sigma})$$

$$+ \sum_{\langle ij \rangle \sigma} t_{\parallel}(p^\dagger_{y,i+a/2,\sigma} p_{y,j+a/2,\sigma} + p^\dagger_{y,i-a/2,\sigma} p_{y,j-a/2,\sigma}) \Big]$$

$$+ h.c. + \sum_{i\mu\sigma}(\epsilon_p n^i_{p_{x(y)},\mu,\sigma} + \epsilon_d n^i_{d\sigma})$$

$$H_1 = U_d \sum_{i\sigma} n^i_{d\sigma} n^i_{d\bar\sigma} + U_p \sum_{i\sigma\mu} n^i_{p_{x(y)},\mu\sigma} n^i_{p_{x(y)},\mu\bar\sigma}$$

$$H_2 = V_{pd} \sum_{i\mu} n^i_d(n^i_{p_x,\mu} + n^i_{p_y,\mu}) + V_{pp} \sum_{i\mu} n^i_{p_x,\mu} n^i_{p_y,\mu}$$

$$+ V_{\parallel} \sum_{\langle ij \rangle \mu} n^i_{p_y,\mu} n^j_{p_y,\mu}$$

where $d^\dagger_{i\sigma}$ creates a hole of spin σ on the copper d-orbital at unit-cell i, $p_{x(y),i\pm a/2,\sigma}$ creates a hole of spin σ at the oxygen p_x (p_y) orbital at sites $\mu = i \pm a/2$ in the x and y directions of unit-cell i. Here $\langle ij \rangle$ corresponds to a sum over nearest-neighbour unit cells i and j and the summation over μ corresponds to $i \pm a/2$. Operator $n^i_{d\sigma}$ is the number operator for the copper atom of unit cell i and $n^i_{p_{x(y)},\mu\sigma}$ are the number operators for the p_x (p_y) orbitals at sites $\mu = i \pm a/2$ of unit cell i. The parameters ϵ_d and ϵ_p are the site-energies of the copper and oxygen sites ($\Delta = \epsilon_d - \epsilon_p$). The copper-oxygen hopping is parametrized by t_{pd} and the oxygen-oxygen hopping by t_{pp} while $t_{\parallel}$ is the hopping between the p_y orbitals of neighbouring unit cells. U_d and U_p are the on-site Hubbard repulsions at the copper and oxygen sites, respectively. The nearest-neighbour copper-oxygen repulsion is parametrized by V_{pd}, the oxygen-oxygen repulsions within a unit cell by V_{pp} and the repulsions between p_y orbitals in neighbouring unit cells by $V_{\parallel}$. Further, the phases of the hopping integrals t, corresponding to the hybridization of d- and p-orbitals are represented in Fig. 2.

We study this model by the DMRG method. The complicated geometry (up to 4th neighbours are connected) of this system required the implementation of a 7-block scheme (Fig. 3). This choice of RG scheme ensures that the relatively complicated geometry, believed to be crucial in the cuprates, is preserved at each step of the calculation. In Fig. 3a, we see the breakup of the two unit-cell system which is the starting point of our calculation. The system size increases by one unit cell (4 sites) at each iteration. The blocks marked '1' and '7' in the figure are renormalized at each iteration and five new blocks (unrenormalized) of one site each are added to the middle of the system. The dimension of the Hilbert space of each of the added sites is 4, corresponding to empty, one hole (up and down spins) and 2 holes. In Fig. 3b, we

represent the blocks and superblocks of the three unit-cell system. The following iterations can be obtained by replacing the superblocks '1' and '7' by the appropriate system. The DMRG method is a highly efficient way to study 1- and quasi 1-dimensional strongly correlated fermionic systems. We are also not limited to a choice of fillings that correspond to closed-shells, a habitual constraint in quantum Monte Carlo simulations.
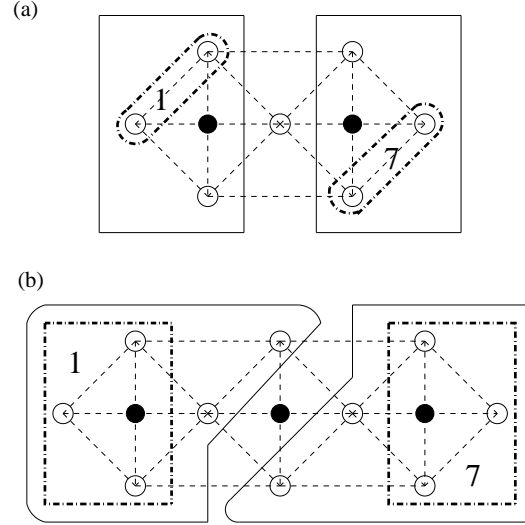

FIG. 3. The breakup of the extended system into blocks and superblocks used in our 7-block DMRG scheme for (a) even iterations and (b) odd iterations. Copper atoms are marked by filled circles and oxygen atoms by open circles. The physical bonds are marked in dashed lines. The superblocks of each iteration are marked in dot-dashed lines and also carry their number (1 and 7). The five central blocks consist of one site each. Superblock sizes increase by two sites in each iteration and the superblock of the following iteration is marked by solid lines.

The parameters varied in our study are mainly the interaction strengths (V's), Δ and the filling. We have studied this model with $t_{pp} = 0.6$, $U_d = 10.0$ and $U_p = 5.0$ in units where $t_{pd} = 1.0$. Further, we consider two different geometries corresponding to values of $t_{\parallel} = 0$ and $t_{\parallel} = 0.6$. The former corresponds to the case of plaquettes that are coupled only at a point (Model 1) and the latter to the case of fully connected plaquettes (Model 2). The choice of parameters for 3-band models of the copper-oxides has been extensively discussed in the literature [21]. Our choice corresponds to quite a realistic range of parameters for the copper oxides [19–21]. In fact, one of the inherent difficulties associated with any study of the copper-oxides is the large number of parameters, giving rise to a huge phase space. We have tried to vary the different V's in order to locate the interesting part of the phase diagram. One of the difficulties encountered in our calculations has been the inaccessibility of certain

ranges of V due to convergence problems, as discussed in the end of Section IIIB.

We have studied up to 25 CuO_3 unit cells, corresponding to 101 sites, at different dopings. Half-filling corresponds to one hole per copper site in the hole picture, where the system is known to be an antiferromagnetic insulator for a wide range of parameter values. We have studied systems with different numbers of holes, corresponding to doping of the physical system. We add two holes at every other iteration. Thus, the filling is not the same at every step of the calculation. The cases we discuss are systems with 20 - 25 unit cells. We have studied systems of N unit cells with n_h holes given by, $n_h = N + 3 + mod(N + 1, 2)$. The filling x is given by $n_h/N - 1$. Thus, $x = 0$ corresponds to the half-filled case. We have studied fillings $x = 0.12$, 0.13 and 0.19 ($N = 25, 23, 21$) for odd numbers of unit cells and $x = 0.17$, 0.18 and 0.25 ($N = 24, 22, 20$) for even numbers of unit cells. Thus, we are able to study a range of doping values. In addition, we have studied the case of $n_h = N + 1 + mod(N + 1, 2)$, for the model with $t_\parallel = 0$.

We compared the ground state energies for several iterations with the energies obtained from exact diagonalization calculations to verify our RG scheme. We varied the number of states m on the superblocks ($m = 125, 150$ and 200). We have kept up to 200 states on the superblocks. This correspond to a Fock space dimension $H_F = m^2 \times 4^5 = 40,960,000$. This provides sufficient accuracy, estimated in several ways. The discarded weight of the density matrix states is of order 10^{-6} with 200 states. In certain cases, we have also calculated the energies and properties of the non-interacting system (free-particle model with all U's and V's set to zero), where exact results are available. This provides a strong check on our data, since convergence is known to be most difficult in this case for the DMRG algorithm. Another property that we have used to check the quality of our data is the magnetic moment $|\langle S_i^z \rangle|$, at site i, which ought to be zero in principle. Thus, only data which correspond to relatively small magnitudes of $|\langle S_i^z \rangle|$ have been used.

III. RESULTS AND DISCUSSION

The physical property we have studied is the current-current (CC) correlation function for links k and l. The current along a bond connecting sites μ and ν is defined as $J_{\mu\nu} = it_{\mu\nu} \sum_\sigma (c_{\mu\sigma}^\dagger c_{\nu\sigma} - c_{\nu\sigma}^\dagger c_{\mu\sigma})$. The mean-field analysis of the 3-band Hubbard model indicated that the nearest-neighbour repulsion V is essential to stabilize the circulating-current phase [2]. The circulating-current phase shown in Fig. 1 would then consist of currents represented by the arrows in the figure. Since we work in the real representation of the Hamiltonian, we use the current-current correlation functions as a measure of this order.

We compared our data for the non-interacting model with the exact data available in this case to assure ourselves of convergence. The current for bond l in unit-cell i is denoted by $J^i(l)$, according to the conventions for bond numbers shown in Fig. 4. We refer to the vertical copper-oxygen bonds as rungs and the horizontal copper-oxygen bonds as legs in analogy to the terminology used for ladders.
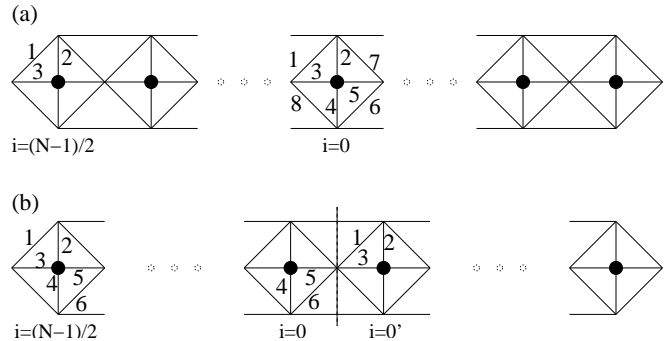

FIG. 4. Conventions for current-current correlation functions studied for systems with (a) odd and (b) even numbers of unit cells. Unit-cell numbers i are marked beneath and the numbers in the figures correspond to the bond numbers.

We have calculated the equal-time, zero-frequency current-current (CC) correlation function, which is the ground state expectation value $\langle J^0(k)J^i(l) \rangle$. These correlations are between currents in the central unit cell, denoted by $J^0(k)$ and currents on the other unit-cells on one half of the system $J^i(l)$ ($i = 1, \ldots (N-1)/2$), for systems with odd numbers of unit-cells. Slightly different correlations are calculated at even and odd iterations due to the DMRG scheme used and these are pictured in Fig. 4. For systems with even numbers of unit-cells, we introduce the notation $\langle J^0(k)J^i(l) \rangle$, and $\langle J^{0'}(k)J^i(l) \rangle$ with $i = 1, \ldots (N-1)/2$, as shown in Fig. 4. However, we continue to refer to both cases as $\langle J^0(k)J^i(l) \rangle$ in the text, with the different notations for even and odd unit-cells being implicit. By the bilateral symmetry about the $O-Cu-O$ axis, it is not necessary to take into account all the possible cases. We therefore restrict ourselves to the case of $\langle J^0(k)J^i(l) \rangle$, $k,l = 1, \ldots 3$. We analyse cases of systems with 20-25 unit-cells, since these are sufficiently large to study the decay of the current-current correlations. In particular, we analyze the behaviour of the different types of diagonal ($\langle J^0(k)J^i(k) \rangle$ and off-diagonal $\langle J^0(k)J^i(l) \rangle$, ($k \neq l$) current-current correlations and try to classify them.

A. Analysis of Model 1

We first present our results for the CC correlations on the CuO_3 system with Model 1 ($t_\parallel = 0$) which consists of plaquettes coupled at a single point. We have performed calculations with values of t_{pd} and t_{pp} equal to 1.0 and 0.6. We have varied Δ and V_{pd}, while V_{pp} was set to 0. We have further considered two sets of fillings corresponding to $n_h = N + 3 + mod(N+1, 2)$ and $n_h = N + 1 + mod(N+1, 2)$. The second series then gives us fillings $x = 0.04$, 0.043 and 0.048 ($N = 25, 23, 21$) and $x = 0.083$, 0.09 and 0.1 ($N = 24, 22, 20$). Thus, the second series $n_h = N + 1 + mod(N+1, 2)$ has the advantage of providing fillings that are practically constant for different system sizes. This helps to verify that our conclusions hold over different system sizes.
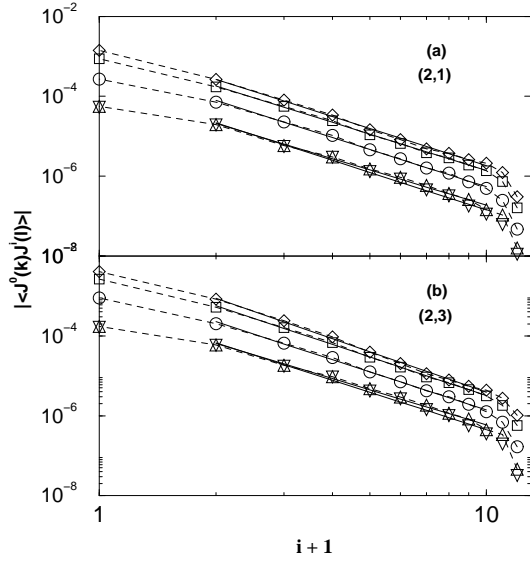

FIG. 5. Current-current correlations $|\langle J^0(k) J^i(l) \rangle|$ for a 25 unit-cell system with 28 holes, for Model 1, in a log-log representation. All systems have the parameters $t_{pp} = 0.6$, $t_\parallel = 0$, $\Delta = 1$ in units with $t_{pd} = 1$. Circles represent the case with the above parameters and all V's = 0, squares are for $V_{pd} = 1$ and diamonds are for $V_{pd} = 2$, all with $U_d = 10$ and $U_p = 5$, obtained from DMRG calculations with $m = 200$ states. Triangles represent the exact values for the correlation for the non-interacting model ($U_p = U_d = V_{pd} = V_{pp} = 0$), and inverted triangles the values obtained for the same parameters from $m = 200$ state DMRG calculations, presented for comparison. Dashed lines are a guide to the eye while full lines correspond to the power-law fits of the data. (a) represents the $|\langle J^0(2) J^i(1) \rangle|$ correlation with $\alpha_{NI}^* = -2.94$, $\alpha_{NI} = -3.12$, $\alpha_0 = -3.09$, $\alpha_1 = -3.03$, $\alpha_2 = -3.09$ and (b) the $|\langle J^0(2) J^i(3) \rangle|$ correlation with $\alpha_{NI}^* = -2.92$, $\alpha_{NI} = -3.11$, $\alpha_0 = -3.16$, $\alpha_1 = -3.21$, $\alpha_2 = -3.37$. See text for definitions of the αs.

We have also carried out numerical fits on our data. For our results on Model 1, we found our data well-fitted by power-laws. We define α_{NI} as the slope corresponding to the non-interacting case obtained from DMRG and α_{NI}^* as the slope of the exact data. Likewise $\alpha_k, k = 0 \ldots 2$ correspond to the cases with $V_{pd} = k$. These slopes give us the exponents of the power-law.

We have studied the effect of increasing the copper-oxygen repulsion V_{pd} on the current-current correlations. In Fig. 4a, we present results for the dependence of the CC correlation function $|\langle J^0(2) J^i(1) \rangle|$ with distance i for a 25 unit-cell system with 28 holes. From Fig. 4, it can be seen that this is the correlation of a rung of the central unit-cell with an oxygen-oxygen bond ($l = 1$) of the unit-cells away from the centre. We first consider this correlation for the non-interacting case (all U's and V's set to 0), where exact results are available. We have compared the results obtained for $|\langle J^0(2) J^i(1) \rangle|$ from a DMRG calculation with $m = 200$ states with the exact results. The convergence of the data is excellent, as seen in Fig. 5a. The exponent of the DMRG data $\alpha_{NI} = -3.12$, compares favorably with the exponent obtained for the exact data, $\alpha_{NI}^* = -2.94$. This is a strong check on our results, since the convergence of the DMRG method is known to be harder for the free-particle model than for the equivalent system with strong correlations.

We now note from Fig. 5a that the curve which represents current-current correlations for the purely local Hubbard model with $U_d = 10, U_p = 5$ and V's = 0, lies above the non-interacting curve. We then turn on nearest-neighbour interactions. Increasing the copper-oxygen repulsion $V_{pd} = 1$ has the effect of increasing the magnitudes of the current-current correlations. Further increasing V_{pd} to 2 increases the correlations, but by a smaller amount. The decay of the correlations follows power-law behaviour, as seen from the log-log plots. Thus, we observe that repulsive interactions are capable of increasing the magnitude of the currents. It can be seen from the curves that the decay at large-distances is hardly affected by the Vs, the curves are nearly parallel. This is borne out by the slopes ($-3.09, -3.03$ and -3.09), which are practically unchanged. This is because the plaquettes are coupled at a single point, which prevents the formation of a state with long-range-order.

In Fig. 5b, we present our results for the correlation $|\langle J^0(2) J^i(3) \rangle|$. This is a correlation between a copper-oxygen rung of the central unit-cell, with a copper-oxygen leg of the side unit-cells. Increasing the copper-oxygen repulsion enhances the magnitude of the correlations compared to the Hubbard model, while their decay is power-law, again with similar exponents, as is seen from the curves which are nearly parallel and from the power-law fits.

In Fig. 6a we present the behaviour of the correlation $|\langle J^0(2) J^i(2) \rangle|$, which is the copper-oxygen rung-rung correlation function. The data presented are for the case of 25 unit-cells with 26 holes, since the absolute magnitude of the correlations is much larger than in the case of 28

holes. The qualitative behaviour remains the same. We observe that the absolute values of the $V_{pd} = 2$ data are enhanced by almost an order of magnitude compared to the $V_{pd} = 0$ curve. We have fitted our data with two series of power-laws for even and odd sites in order to take into account the alternating behavior of the curves. The slight differences between α_0 and α_1 can be attributed to the rather large alternance of the $V_{pd} = 0$ data. This alternance is reminiscent of the generic behavior of correlation functions in quasi-1D systems, due to the harmonics of k_F. We notice that the magnitude of the oscillations decreases when V is increased. In quasi-1D systems, similar behavior of spin-spin and charge-charge correlations is interpreted as an increase in the value of the charge-stiffness (K_ρ) [22].
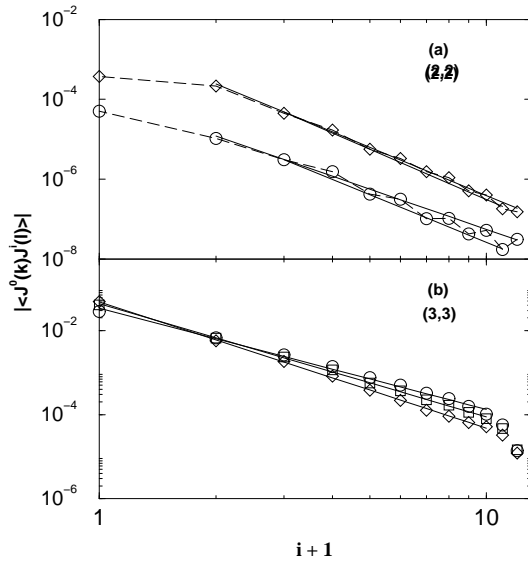

FIG. 6. Current-current correlations for a 25 unit-cell system for Model 1. Note the log-log presentation. All systems have the parameters ($t_{pp} = 0.6$, $t_\parallel = 0$, $\Delta = 1$, $U_d = 10$, $U_p = 5$). Circles represent the case with the above parameters and all V's $= 0$, squares are for $V_{pd} = 1$ and diamonds are for $V_{pd} = 2$. Dashed lines are a guide to the eye, while full lines represent the power-law fits. (a) $|\langle J^0(2)J^i(2)\rangle|$ for a 25 unit-cell system with 26 holes with ($\alpha_0 = -3.34$ (even) and -3.94 (odd)); ($\alpha_1 = -4.00$ (even) and -4.18 (odd)). and (b) $|\langle J^0(3)J^i(3)\rangle|$ for a 25 unit-cell system with 28 holes with ($\alpha_0 = -2.40$, $\alpha_1 = -2.69$, $\alpha_2 = -3.00$).

The behaviour of the correlations $|\langle J^0(3)J^i(3)\rangle|$ can be seen in Fig. 6b. This correlation is a copper-oxygen leg-leg correlation function, as seen from Fig. 4. Here, the behaviour observed is different from the previous cases studied, since the correlation is enhanced very slightly by increasing repulsions for first neighbours. However, the situation is reversed at very short distances and increasing repulsions causes the correlations to decay even faster, as can be noted from the crossing of the curves

in Fig. 6b. Their decay is power-law with the exponents decreasing, as can be seen from the figure.

We have also analysed the behaviour of correlation functions of the type $|\langle J^0(1)J^i(1)\rangle|$. These are not presented for reasons of space. These correlations are oxygen-oxygen correlations and decay as power-laws, with the magnitudes falling as V_{pd} is increased. This however, could be due to the value of $V_{pp} = 0$, chosen here.

We now briefly discuss the case of $x = 0.18$ (22 unit-cells with 26 holes), which fits into the above analysis with an interesting reversal. In this case, the rung-rung correlations (indeed, correlations involving one rung) are initially decreased when V_{pd} is turned on. Increasing V_{pd} to 2 brings about a reversal of this behaviour, with the magnitude of the correlations increasing compared to the $V_{pd} = 0$ case. In Fig. 7 we present one example of this behaviour with the correlation $|\langle J^{0'}(2)J^i(3)\rangle|$, which is a rung-leg correlation. The reversal of the trend is clearly seen from the $V_{pd} = 1$ curve (lies below the $V_{pd} = 0$ curve) and the $V_{pd} = 2$ data which is enhanced with respect to the $V_{pd} = 0$ curve. This indicates that there could be a threshold value of nearest-neighbour interactions V for enhancing the magnitude of current-current correlations.
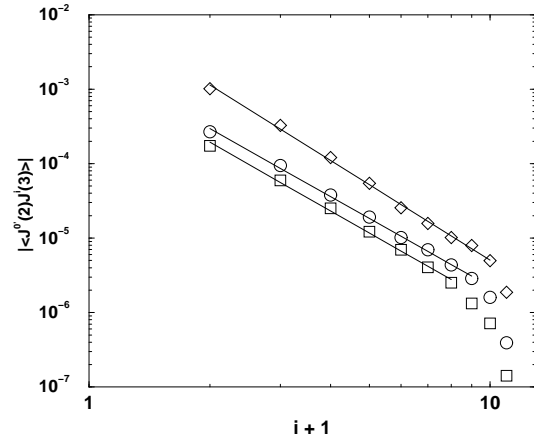

FIG. 7. Current-current correlations $|\langle J^{0'}(2)J^i(3)\rangle|$ for a 22 unit-cell system with 24 holes. Note the log-log representation. All systems have the parameters ($t_{pp} = 0.6$, $t_\parallel = 0$, $\Delta = 1$, $U_d = 10$, $U_p = 5$) Circles represent the case with the above parameters and all V's $= 0$, squares are for $V_{pd} = 1$, diamonds for $V_{pd} = 2$. Lines represent power-law fits with exponents $\alpha_0 = -2.41$, $\alpha_1 = -2.69$ and $\alpha_2 = -3.00$.

Thus, the above analyses show that the copper-oxygen rung-rung correlation (or even correlations involving one rung) are enhanced in magnitude by repulsive interactions, compared to the purely local Hubbard model, probably requiring a minimum threshold value of V. The copper-oxygen leg-leg correlations show an initial increase followed by a decay in magnitude and correlation

length, as V_{pd} is increased. The oxygen-oxygen correlation is diminished in magnitude and correlation length, as V_{pd} is increased. We have analysed the cases of different fillings described above and have found similar behaviour in all these cases.

B. Analysis of Model 2

We now turn to an analysis of Model 2 with $t_\| = 0.6$, The behavior of this model is expected to be quite different from that of the $t_\| = 0$ case. It is expected that the long-distance behavior of the CC correlations is much more sensitive to the nearest-neighbour repulsions V. Here, we first study the purely local Hubbard model on our lattice ($U_d = 10$, $U_p = 5$ and $V's = 0$). We note that this corresponds to the system in Fig. 2c, with bonds connecting different plaquettes ($t_\| = 0.6$). However, the V on this bond is initially set to zero, to give us a model of connected plaquettes with purely local interactions. We the begin to turn on Vs, i.e we turn on copper-oxygen and oxygen-oxygen nearest-neighbour interactions, along with the interaction $V_\|$ ($V_{pd} = V_{pp} = V_\| = 1.0$). Thereafter, we further increase $V_\|$ to study the effect of longer-range interactions on the current-current correlations.

We shall first consider the case of 25 unit cells at a filling of 0.12 in some detail before analysing our other data. In Fig. 8a - 8c we present diagonal correlations of the type $|\langle J^0(k)J^i(k)\rangle|$, for $k = 1, \ldots 3$, on a log-log scale. These correspond respectively to the oxygen-oxygen diagonal correlation, the rung-rung correlation and the leg-leg correlation of bonds in the central unit cell with bonds in the side unit cells. In Fig. 8a, we present the decay of the oxygen-oxygen diagonal correlation ($|\langle J^0(1)J^i(1)\rangle|$) with increasing distance for increasing values of the nearest-neighbour repulsion V. These are compared to the data with all V's = 0, i.e. the purely local Hubbard model. From the data in Fig. 8a, we note the effect of repulsions on the correlations between currents on oxygen-oxygen bonds. Turning on V's, ($V_{pd} = V_{pp} = V_\| = 1$) causes the correlations to decay in magnitude compared to the Hubbard model. Further increasing $V_\|$ to 3, causes the correlations to decay further. Data for $V_{pd} = V_{pp} = 1, V_\| = 2$, fit smoothly into this pattern and have not been shown, for clarity. The correlations show exponential decay as can be seen from the plots as well as the inset. We have fitted the Hubbard model curve and the $V_\| = 3$ data (scaled by a factor of 10) by expressions of the form $y = A\,exp(\beta x)$, shown in the inset. The clear straight lines seen in the semilog plot are indicative of the quality of the fit. We obtain $A = -6.0065$ and $\beta = -0.6296$ for the Hubbard model (Vs = 0) and $A = -3.3280$ and $\beta = -0.7753$ for the $V_\| = 3$ data.
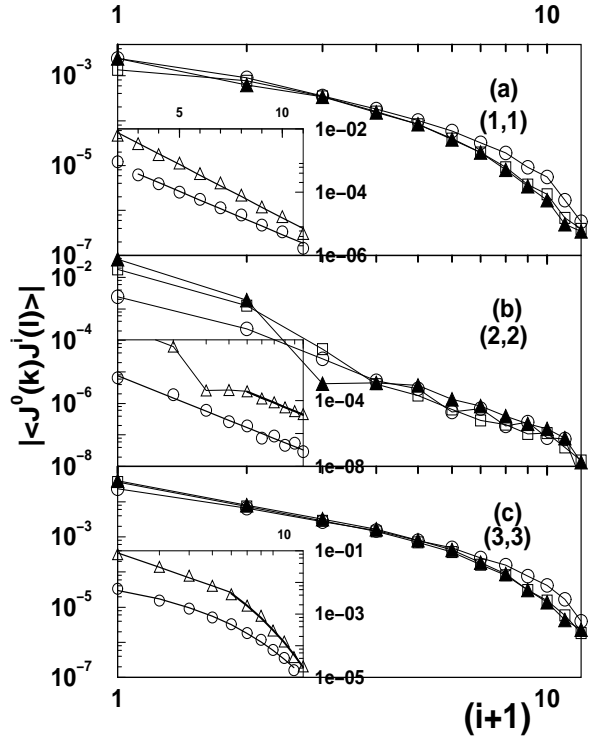

FIG. 8. Diagonal current current correlations for a 25 unit-cell system with 28 holes ($|\langle J^0(k)J^i(k)\rangle|$) in a log-log representation. All systems have the parameters ($t_{pp} = t_\| = 0.6$, $\Delta = 1$, $U_d = 10$, $U_p = 5$) in units with $t_{pd} = 1$. Circles represent the case with the above parameters and all V's = 0, squares are for $V_{pd} = V_{pp} = V_\| = 1$, triangles for $V_{pd} = V_{pp} = 1, V_\| = 3$. Triangles are in some cases filled, for clarity. Lines in the main figures are meant to be a guide to the eye. Lines in the insets correspond to fits which are discussed in greater detail in the text. From top to bottom, (a) diagonal oxygen-oxygen correlation function $|\langle J^0(1)J^i(1)\rangle|$. Inset (semilog representation) contains $V_\| = 3$ data multiplied by a factor 10, for visibility. (b) rung-rung correlation $|\langle J^0(2)J^i(2)\rangle|$. The inset (log-log plot) contains $V_\| = 3$ data multiplied by a factor 100. (c) leg-leg correlation $|\langle J^0(3)J^i(3)\rangle|$. The inset (log-log plot) contains $V_\| = 3$ data multiplied by a factor 10.

In Fig. 8b we present correlations of type $|\langle J^0(2)J^i(2)\rangle|$, which correspond to the copper-oxygen rung-rung correlation, for different values of interaction strengths. Here, we notice a sizeable enhancement of the current-current correlations (by an order of magnitude) over distances of a few lattice spacings as interactions (V's) are turned on, compared to the Hubbard model. Thereafter, interactions cause the correlations to fall, with respect to the V's = 0 case. However, further increasing $V_\|$ causes the correlations to rise i.e. there is a reversal of the trend. It is reassuring that the DMRG data in these cases are well converged, as seen from the small discarded weight and the small magnetic moments at the central sites, $|S_i^z| \leq 4\times10^{-4}$. These data have been fitted by power-laws. The fits are good as seen from the

straight-lines in the log-log plots, both in the main figure and in the inset (thick lines correspond to the fits). The slope of the straight line gives the exponent of the power-law and we obtain $\alpha_0 = -4.4070$ and $\alpha_3 = -4.6830$. We also note that the cross-rung-rung correlation, of type $|\langle J^0(2)J^i(4)\rangle|$ are similar qualitatively and quantitatively to the rung-rung correlations and are not presented here.

In Fig. 8c we present correlations of type $|\langle J^0(3)J^i(3)\rangle|$, which correspond to the copper-oxygen leg-leg correlation, for different values of interaction strengths. Here, we notice a slight enhancement of the current-current correlations over distances of a few lattice spacings as interactions (V's) are turned on, compared to the Hubbard model. Thereafter, interactions cause the correlations to fall, with respect to the V's = 0 case, upon increasing Vs. The long-distance behaviour in this case is interesting. The $V = 0$ data (Hubbard model) are clearly exponential as seen from the main figure and the inset ($A = -3.9204$ and $\beta = -0.6254$). On the other hand the $V_\parallel = 3$ data (triangles) show much more complex behaviour corresponding to power-law behavior at short distances (up to 6 sites) followed by an exponential tail at long distances. The power-law fit is indicated in the inset by the thin line and the exponential tail by the thick line. We obtain the power-law exponent $\alpha_3 = -2.6299$ from the slope of the power-law part of the fit and $A = -0.0143$ and $\beta = -0.8947$ for the exponential part (thick line).

We now turn to an analysis of the off-diagonal correlations. Given the large number of correlations, we attempt to set out the general trends by treating one off-diagonal correlation of each type. In Fig. 9a - Fig. 9c, we present off-diagonal CC correlations, $|\langle J^0(1)J^i(2)\rangle|$, $|\langle J^0(3)J^i(2)\rangle|$ and $|\langle J^0(3)J^i(1)\rangle|$. The first of these corresponds to the correlation of an oxygen-oxygen bond in the central unit-cell with copper-oxygen rungs of the side unit cells. We refer to this henceforth as an "oxygen-rung" correlation. As seen from the log-log plot of Fig. 9a, the correlation (1,2) exhibits power-law decay both for the Hubbard model and upon increasing Vs. There is a substantial increase of this correlation at short distances with increasing V. This trend persists over long distances for the case of $V_\parallel = 3$ as seen from the figure. The power-law fits to these data are presented in the inset, with the $V = 3$ data scaled by a factor 10. We have fitted the Hubbard model data in two series corresponding to the odd and even points to take care of the alternance present in our data and obtain α_0s of -3.9408 (odd) and -3.3321 (even). The $V_\parallel = 3$ data were fitted by a power-law with exponent $\alpha_3 = -4.0923$. We note that the alternance of the $V_\parallel = 3$ is strongly diminished with respect to the $V = 0$ data.

Similar behavior is observed in the leg-rung correlation function $|\langle J^0(3)J^i(2)\rangle|$, presented in Fig. 9b. The $V_\parallel = 3$ data are clearly enhanced with respect to the Hubbard model data almost over all the length of the curve. We

followed a procedure similar to the previous case, fitting the $V = 0$ data by power-laws in two series to obtain α_0s of -3.0559 (odd) and -4.0292 (even). The power-law fits to the $V_\parallel = 3$ data gave us an exponent α_3 of -4.1966. Correlations quench the even-odd alternation of the data.
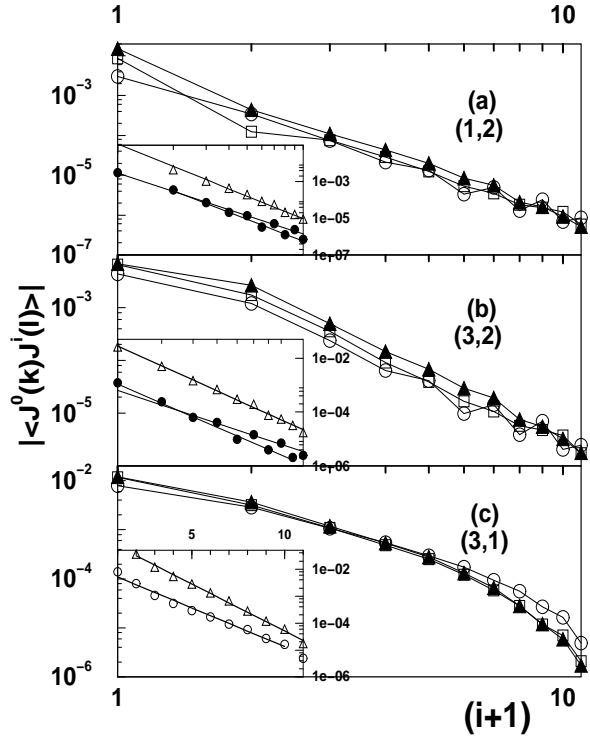

FIG. 9.   Off-diagonal current current correlations $|\langle J^0(k)J^i(l)\rangle|$ ($k \neq l$) for a 25 unit-cell system with 28 holes in a log-log representation. All systems have the parameters ($t_{pp} = t_\parallel = 0.6$, $\Delta = 1$, $U_d = 10$, $U_p = 5$) in units with $t_{pd} = 1$. Circles represent the case with the above parameters and all V's = 0, squares are for $V_\parallel = V_{pp} = V_\parallel = 1$, triangles for $V_{pd} = V_{pp} = 1, V_\parallel = 3$. Symbols are in some cases filled, for clarity. Lines in the main figures are meant to be a guide to the eye. Lines in the insets correspond to fits which are discussed in greater detail in the text. From top to bottom, (a) "oxygen-rung" correlation $|\langle J^0(1)J^i(2)\rangle|$. Inset (log-log) contains $V_\parallel = 3$ data multiplied by a factor 10, for visibility. (b) leg-rung correlation $|\langle J^0(3)J^i(2)\rangle|$. The inset (log-log plot) contains $V_\parallel = 3$ data multiplied by a factor 10. (c) "leg-oxygen" correlation $|\langle J^0(3)J^i(1)\rangle|$. The inset (semilog plot) contains $V_\parallel = 3$ data multiplied by a factor 10.

In Fig. 9c, we present the correlation $|\langle J^0(3)J^i(1)\rangle|$, which corresponds to the correlation of the central oxygen-oxygen bond with the copper-oxygen leg of the side unit cell. We refer to this correlation henceforth as the "oxygen-leg" correlation. We observe from the figure and from the fits in the inset that these correlations have exponential behavior for the Hubbard model as well as for the case with $V_\parallel = 3$. From the fits seen in the inset (presented in semilog form) we obtain $A = -4.61476$ and

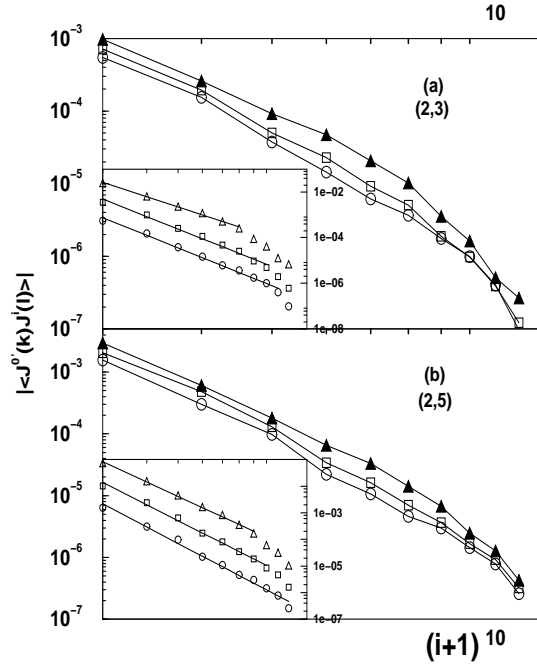$\beta = -0.6600$ for the $V = 0$ case and $A = -1.849094$ and $\beta = -0.8081$ for the $V_\parallel = 3$ case.

FIG. 10. Current-current correlations $|\langle J^{0'}(2)J^i(k)\rangle|$ for a 22 unit-cell system with 26 holes. All systems have the parameters $t_{pp} = t_\parallel = 0.6$, $\Delta = 1$, $U_d = 10$, $U_p = 5$ in units with $t_{pd} = 1$. Circles represent the case with the above parameters and all V's $= 0$, squares are for $V_{pd} = V_{pp} = V_\parallel = 1$ and triangles for $V_{pd} = V_{pp} = 1, V_\parallel = 3$. Triangles are in some cases filled, for clarity. Lines in the main figures are meant as a guide to the eye and lines in the insets are the power-law fits to the data. In both insets, $V_\parallel = 1$ data (squares) is multiplied by a factor of 5 and $V_\parallel = 3$ data (triangles) by a factor of 25 for clarity. From top to bottom, (a) rung-leg correlation, $|\langle J^{0'}(2)J^i(3)\rangle|$. From the fits, $\alpha_0 = -4.4157$, $\alpha_1 = -4.3648$ and $\alpha_2 = -3.5904$. (b) another rung-leg correlation $|\langle J^{0'}(2)J^i(5)\rangle|$. From the fits, $\alpha_0 = -4.9475$, $\alpha_1 = -4.7718$ and $\alpha_2 = -4.3446$.

In addition to the data presented in Figs. 8-9, for the 25 unit-cell system with filling $x = 0.12$, we discuss some results for the case of 22 unit-cells with $x = 0.18$. In Fig. 10, we present the evolution of two types of rung-leg correlations that are similar: $|\langle J^{0'}(2)J^i(3)\rangle|$ and $|\langle J^{0'}(2)J^i(5)\rangle|$, henceforth referred to as the $(2', 3)$ and $(2', 5)$ correlations respectively. In Fig. 10a, we see that the $V_\parallel = 1$ data of the $(2', 3)$ correlation is already enhanced with respect to the Hubbard model data over intermediate distances. The $V_\parallel = 3$ data is clearly enhanced with respect to the Hubbard model data. We have fitted these data by means of power-laws, as seen from the log-log scale of the curve. The results of the fits are seen from the inset. We see that α_3, the exponent of the $V_\parallel = 2$ curve is visibly reduced to -3.59 compared

to $\alpha_0 = -4.94$ for the Hubbard model and the $V_\parallel = 3$ data falls off much more slowly than the Hubbard model data. As seen from the inset, the number of points we were able to include in the fit decreases with increasing V, as compared to the Hubbard model. It is accepted that convergence of the DMRG algorithm is best in the presence of strong, local interactions. Our Hubbard model case falls into this category with $U_d = 10$ and $U_p = 5$. Increasing V clearly renders convergence much more difficult, especially when $V_\parallel = 3$ which is most probably the reason for this behavior.

In Fig. 10b, we present in a manner analogous to Fig. 10a, data for the $(2', 5)$ correlation functions. As in the previous case, we note that the $V_\parallel = 3$ data is stabilized compared to the $V = 0$ data and the $V_\parallel = 1$ data, with the exponents $\alpha_0 = -4.9475$, $\alpha_1 = -4.7718$ and $\alpha_3 = -4.3446$. Thus, we note that the decay of the $(2', 5)$ correlation is slower for $V_\parallel = 3$ than for the Hubbard model. We have dropped 3 points from the $V_\parallel = 3$ curve and 1 point from the Hubbard model curve to obtain these results.

Thus, the analysis of the diagonal and off-diagonal CC correlation functions of Model 2 yields the following trends : the nearest-neighbor repulsive interaction V is clearly capable of increasing the magnitude of the current-current correlations locally and of strongly modifying the long-distance behavior. The correlations fall into different categories.

The rung-rung correlation function is enhanced by increasing Vs and shows power-law decay. In certain cases, the exponent of the power-law decreases upon increasing V and the correlations fall off slowly as compared to the Hubbard model. In fact, this extends to any correlation that includes at least one rung, diagonal or off-diagonal.

The leg-leg correlations show exponential decay in the Hubbard model. However, increasing the values of Vs and $V_\parallel$ in particular changes this behaviour - we now have a power-law behavior at short distances followed by an exponential tail. Thus, we see that Vs are capable of locally enhancing the CC correlations and by connecting the plaquettes, the long-distance behaviour is greatly modified. We believe that the difference between the rung-rung and leg-leg correlations is due to our choice of model and that this difference should disappear in the 2D system.

The oxygen-oxygen correlation function shows exponential decay with very slight enhancement of the absolute values for $V_\parallel = 3$. This is also true of the "oxygen-leg" type correlation functions. This could however be due to our choice of parameter values. Clearly, it would be interesting to study other parameter ranges for the Vs, especially for V_{pd} and V_{pp}. This point is discussed further down in this section.

We have studied various cases involving other parameter values. Notably, we tried to increase V_{pd} and V_{pp} ($V_{pd} = 2.0$, 3.0, $V_{pp} = 2.0$, in units of t_{pd}), but encountered

convergence problems at the level of the Lanczos diagonalization algorithm. It is quite likely that increased degeneracy of the ground state slows down convergence, as is known to occur in other cases such as the $J_1 - J_2$ spin chain, at parameter values close to the critical point. This is most probably due to the increased delocalization of the ground state, brought about by larger V's. To overcome this problem, it would be necessary to increase the number of states m that we keep on the superblocks. However, at our present value of $m = 200$, we are already at the limit of our computational resources. The charge densities in our systems show that the charges tend to be concentrated on the copper atoms, which possibly competes with the stabilization of currents. Thus, increasing V_{pd} and V_{pp} is likely to bring about a rehomogenization of charge and this could be favourable to the current-current correlations.

At this juncture, it is interesting to compare the models with $t_\parallel = 0$ and 0.6. We have observed enhancement in the magnitudes of the currents in both models. Thus, repulsive nearest-neighbour interactions are clearly capable of increasing the magnitudes of currents. The long-distance behaviour of correlations is different in the two models. Model 1 shows power-law decay of correlations and the interaction V has a very small effect on the exponents. In Model 2, any correlation involving a rung shows power-law behaviour. We have very interesting indications that repulsive nearest-neighbour interactions can enhance currents over distances comparable to the length scale of the system. In certain cases, the exponent is considerably reduced and the current-current correlations stabilized compared to the Hubbard model.

IV. CONCLUSIONS

In conclusion, we have studied a 3-band extended Hubbard Hamiltonian on a model CuO_3 system, with geometry similar to that of a section of the CuO_2 planes of the copper-oxides. We have studied two different cases, with the parameter $t_\parallel = 0$ and 0.6, which correspond respectively to Model 1 with plaquettes coupled at a single point and Model 2, with plaquettes coupled all along the length of the system. Our calculations show that nearest-neighbour repulsive interactions are clearly capable of enhancing current-current correlations in magnitude and of qualitatively changing the long-distance behavior of the system. Model 1 shows power-law decay of correlations and the interaction V_{pd} has a very small effect on the exponents. Increasing the copper-oxygen repulsion V_{pd} can increase the magnitude of the rung-rung current-current correlation (or correlations involving a single rung) by up to an order of magnitude. In Model 2, the effect of introducing nearest-neighbour interactions V in the system is to produce a sizeable increase in the rung-rung correlations over distances of a few lattice spacings. $V_\parallel$

can enhance correlations involving at least one copper-oxygen rung over distances comparable to the length of the system. In certain cases, interactions bring about a sizeble decrease in the exponent, causing the correlations to decay slowly with respect to the Hubbard model. We have indications that threshold values of the nearest-neighbour repulsions are necessary to observe stabilization at long distances. Tuning the copper-oxygen and the oxygen-oxygen repulsions would redistribute charge more uniformly in the system which is likely to stabilize the current-current correlation functions in this system. We believe that the enhancement and stabilization of certain correlation functions seen in our model constitutes a trend that will hold for the 2D system.

[1] for a recent experimental survey of the pseudogap phase, see, T. Timusk and B. Stratt, Rep. Prog. Phys. **62**, 61 (1999) and references therein.

[2] C. M. Varma, Phys. Rev. B **55**, 14554 (1997); Phys. Rev. Lett. **83**, 3538 (1999); Phys. Rev. B **61**, 3804 (2000).

[3] S. Chakravarty, R. B. Laughlin, D. K. Morr and C. Nayak, Phys. Rev. B **63**, 094503 (2001).

[4] B. I. Halperin and T. M. Rice, Solid State Phys. **21**, 116 (1968).

[5] H. J. Schulz, Phys. Rev. B **39**, 2940 (1989).

[6] I. Affleck and J. B. Marston, Phys. Rev. B **37**, 3774 (1991).

[7] T. D. Stanescu and P. Phillips, Phys. Rev. B **64**, 220509 (2001).

[8] D. A. Ivanov, P. A. Lee and X-G. Wen, Phys. Rev. Lett. **84**, 3958 (2000).

[9] P. W. Leung, Phys. Rev. B **62**, R6112 (2000).

[10] D. J. Scalapino, S. R. White and I. Affleck, Phys. Rev. B **64**, 100506 (2001).

[11] J. O. Fjaerestad and J. B. Marston, Phys. Rev. B **65** 125106 (2002).

[12] J. B. Marston, J. O. Fjaerestad and A. Sudbo, to be published in Phys. Rev. Lett.

[13] E. Dagotto, Rev. Mod. Phys. **66**, 763 (1994).

[14] P. B. Littlewood, C. M. Varma and E. Abrahams, Phys. Rev. Lett. **60**, 379 (1987), C. M. Varma, S. Schmitt-Rink and E. Abrahams, Solid State Commun. **62**, 681 (1987).

[15] V. J. Emery, Phys. Rev. Lett. **58**, 2794 (1987).

[16] S. R. White, Phys. Rev. B **48**, 10345 (1993).

[17] E. Orignac and T. Giamarchi, Phys. Rev. B **56**, 7167 (1997).

[18] H-H. Lin, L. Balents and M. P. A. Fisher, Phys. Rev. B **48**, 10345 (1993).

[19] M. Guerrero, J. E. Gubernatis and S. Zhang, Phys. Rev. B **57**, 11980 (1998).

[20] Z. B. Huang, H. Q. Lin and J. E. Gubernatis, Phys. Rev.

B **63**, 115112 (2001).

[21] M. S. Hybertson, M. Schlüter and N. E. Christensen, Phys. Rev. B **39**, 9028 (1989); A. K. McMahan, J. F. Annett and R. L. Martin, Phys. Rev. B **42**, 6268 (1990); R. L. Martin, Phys. Rev. B **53**, 15501 (1996).

[22] F. D. M. Haldane, J. Phys. C **14**, 2585 (1996); T. Giamarchi and H. J. Schulz, Phys. Rev. B **39**, 4620 (1989).